INSTITUTE OF PHYSICS PUBLISHING PLASMA SOURCES SCIENCE AND TECHNOLOGY
Plasma Sources Sci. Technol. **11** (2002) 248–253 PII: S0963-0252(02)35989-9

Spatial profiles of N_2^+ concentration in an atmospheric pressure nitrogen glow discharge

A P Yalin[1,2], C O Laux[1], C H Kruger[1] and R N Zare[2]

[1] Department of Mechanical Engineering, Stanford University, Stanford, CA 94305, USA
[2] Department of Chemistry, Stanford University, Stanford, CA 94305, USA

E-mail: ayalin@stanford.edu

Received 4 March 2002, in final form 8 April 2002
Published 17 May 2002
Online at stacks.iop.org/PSST/11/248

Abstract
Spatial profiles of N_2^+ concentration are measured in an atmospheric pressure nitrogen glow discharge by cavity ring-down spectroscopy. At discharge currents of ∼100 mA, we measure centreline ion concentrations on the order of 10^{12} cm^{-3}, and radial profiles with radial-half-maximum of ∼1 mm. The measurements have sub-ppm concentration sensitivity, and sub-millimetre spatial resolution. Using a collisional–radiative model we relate the ion concentrations to electron number densities, and we find good agreement with spatially integrated electrical measurements. The measured concentrations indicate significant nonequilibrium in the discharges.

1. Introduction

Atmospheric pressure glow discharges are of interest as plasma sources for applications including biochemical decontamination, remediation of toxic gases, material processing and electromagnetic wave shielding. A characteristic of glow discharges is that the electron temperature T_e is elevated with respect to the temperature T_g of the heavy species. Similar glow discharges have been studied in our laboratory, and we find representative parameters are $T_e \sim 10\,000$ K and $T_g \sim 2000$–4000 K [1, 2]. At these conditions, energetic electrons produce a significant degree of ionization and dissociation. Thus, the nonequilibrium glow discharges have elevated electron and excited state populations, making them attractive as potential active sources for the aforementioned applications.

Measurements of ion and/or electron number density are needed to characterize experiments and validate models. Physical probes tend to disturb the system, and techniques such as Thomson scattering and interferometry do not readily provide results with high spatial resolution. Optical techniques that measure ion concentrations are widely used. Of these, emission provides information only on excited species, fluorescence suffers from quenching effects and optical interference that complicate interpretation, and absorption often lacks sensitivity. Cavity ring-down spectroscopy (CRDS), on the other hand, is a sensitive line-of-sight laser absorption technique that has been used to measure species concentrations in low-pressure plasmas [3–7]. In particular, the N_2^+ ion has been studied in low-pressure hollow cathode sources [8, 9]. Here, we use CRDS to record spatial profiles of N_2^+ concentration in an atmospheric pressure nitrogen glow discharge. A collisional–radiative (CR) model is used to compute population fractions and to relate the measured ion concentrations to electron number densities. The inferred electron number density profiles are compared with electrical measurements, and the nonequilibrium nature of the plasma is discussed.

2. Cavity ring-down spectroscopy

CRDS has become a widely used method in absorption spectroscopy owing primarily to its high sensitivity. Detailed reviews of the technique may be found in [10, 11]. Essentially, a laser beam is coupled into a high-finesse optical cavity containing a sample, where it passes many times between the mirrors. As the light bounces back and forth inside the cavity, its intensity decays (rings down) owing to sample absorption, particle scattering loss (generally negligible), and mirror transmission loss. A photodetector is used to measure the ring-down signal, which is fitted to yield the sample loss. The technique affords high sensitivity owing to a combination of long effective path length and insensitivity to laser energy

 © 2002 IOP Publishing Ltd Printed in the UK

fluctuations, and therefore is well suited to the detection of trace species in plasmas. Under appropriate conditions, the ring-down signal $S(t)$ decays exponentially [12, 13]:

$$S(t) = S_0 \exp\left(-\frac{t}{\tau}\right),$$
$$\frac{1}{\tau} = \frac{c}{l}[l_{\text{abs}} k_{\text{eff}}(\nu_{\text{L}}) + (1 - R)]; \quad (1)$$
$$k_{\text{eff}}(\nu_{\text{L}}) \equiv \int_{-\infty}^{+\infty} \mathrm{d}\nu\, L(\nu - \nu_{\text{L}}) k(\nu)$$

where τ is the 1/e time of the decay (termed the ring-down time), c is the speed of light, l is the cavity length, l_{abs} is the absorber column length, $k_{\text{eff}}(\nu)$ is the effective absorption coefficient, ν_{L} is the laser frequency, $1 - R$ is the effective mirror loss (including scattering and all cavity losses), $L(\nu)$ is the laser lineshape function, and $k(\nu)$ is the absorption coefficient. The effective absorption coefficient accounts for line broadening arising from the laser lineshape. Generally, the measured ring-down signal is fit with an exponential, and the ring-down time τ is extracted. Combining τ with the ring-down time τ_0 measured with the laser detuned from the absorption feature allows a determination of the sample absorbance, and hence effective absorption coefficient

$$\text{Abs} \equiv l_{\text{abs}} k_{\text{eff}}(\nu_{\text{L}}) = \frac{l}{c}\left[\frac{1}{\tau} - \frac{1}{\tau_0}\right]. \quad (2)$$

We circumvent the laser lineshape dependence by tuning the laser frequency across an absorption line, and measuring the frequency-integrated absorption coefficient. By definition, the frequency-integrated absorption coefficient is the same as the frequency-integrated effective absorption coefficient, and is easily related to the strength of the given absorption line and species concentration.

Because CRDS is a line-of-sight technique, its spatial resolution depends on the symmetry of the sample. In cases where the sample varies only in directions perpendicular to the optical axis, the resolution is determined by the spatial profile of the laser beam in the cavity, which depends on transverse mode coupling [10, 11]. In cases such as ours, where an axisymmetric sample is probed with the optical axis aligned perpendicularly to the sample's symmetry axis, an Abel inversion technique can be used to recover the radial profile of the sample. Then, assuming the beam waist is sufficiently small compared to the characteristic dimension of the sample, the resulting spatial resolution is determined by the spatial step-size and the accuracy of the Abel inversion.

3. Experimental section

3.1. Discharge

Similar discharges to the one studied in this work have previously been described in detail [1]. A photograph of the atmospheric pressure nitrogen discharge with a schematic representation of the ring-down cavity is shown in figure 1. Nitrogen is injected through a flow straightener and passes through the discharge region with a velocity of $\sim$20 cm s^{-1}. The discharge is formed between a pair of platinum pins (separation 0.85 cm) that are vertically mounted on water-cooled stainless-steel tubes. The discharge is maintained by a DC current supply ($i_{\text{max}} = 250$ mA) in a ballasted circuit ($R_{\text{b}} = 9.35$ kΩ). The pins are brought together to ignite the discharge, and are then separated using a translation stage. The position of the discharge is observed to be stable and reproducible. The discharge is contained within a Plexiglas cylinder (diameter 12″) that isolates it from room air disturbances. Small holes allow weak ventilation by a fan through the top to avoid accumulation of undesirable by-products of the discharge (such as ozone or oxides of nitrogen), and enable passage of the laser beam through the discharge. A second translation stage is used to displace the entire discharge cylinder relative to the optical axis in order to obtain spatial profiles.

3.2. Optical

We study the N_2^+ ion by probing the (0, 0) band of its first negative system ($B\,^2\Sigma_u^+$–$X\,^2\Sigma_g^+$) in the vicinity of 391 nm. We select this spectral feature because it is comparatively strong and optically accessible. The optical layout is shown in figure 2. An OPO system (doubled idler) is used as the light source (repetition rate = 10 Hz, pulse width $\sim$7 ns, pulse energy $\sim$3 mJ, linewidth $\sim$0.14 cm^{-1}). The output from the OPO passes through a Glan–Taylor polarizer to attenuate the energy, and several beam shaping optics to approximately mode-match the beam into the cavity. We use a linear cavity of length 75 cm with 50 cm radius-of-curvature (ROC) mirrors. The selection of cavity geometry is discussed below. Typically, about 100 μJ per pulse is incident on the back face of the entrance ring-down mirror. The ring-down

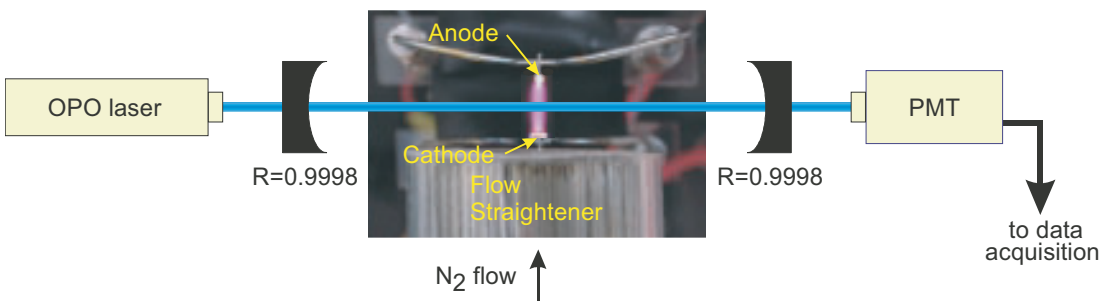

Figure 1. Photograph of the atmospheric pressure nitrogen discharge and schematic diagram of the ring-down cavity: electrode separation 0.85 cm, discharge current 187 mA.

signal is collected behind the output mirror with a fast photomultiplier tube (Hammamatsu-R1104), which we filter against the pump laser and other luminosity with two narrow-band interference filters (CVI-F10-390-4-1). The PMT signals are passed to a digitizing oscilloscope (HP 54510A, 250 MHz analog bandwidth, eight-bit vertical resolution) and are read to computer with custom data acquisition software. In a typical ring-down spectrum, 16 or 32 decay curves are averaged at each wavelength, and the resulting waveform is fitted with an exponential to yield the ring-down time τ. The portion of the ring-down signal used in the fit is that in between 90% and 10% of the peak (initial) signal amplitude. The detuned ring-down time τ_0 is determined with the laser tuned off the absorption features. Spectral scans use a step-size of 0.001 nm. When performing spatial scans, we use step-sizes of 0.2 mm.

Implementing CRDS in the atmospheric plasma requires special care in the choice of cavity geometry. For a linear cavity formed with mirrors of equal ROC, the cavity geometry is determined by the dimensionless g-parameter, defined as unity minus the cavity length divided by the mirror radius of curvature [14]. Initial attempts to form a ring-down cavity with $g = 0.875$ (length 75 cm, 6 m ROC mirrors), resulted in distorted and irreproducible profiles, owing to beam steering from index-of-refraction gradients (similar to a mirage). We verified that this was the case by using a Watec-902C CCD camera to image the light exiting the cavity [15]. With the cavity aligned and the plasma discharge off, the CCD camera image shows a single spot, indicating that the beam is incident on the rear mirror at the same location on each pass. With the plasma ignited, the image on the camera changed to multiple spots, corresponding to the beam walking within the cavity. Recent work by Spuler *et al* [16] simulates the effect of cavity geometry on beam propagation in CRDS experiments. Their results indicate that a g-parameter of about -0.5 represents a good compromise between beam waist and beam walk in environments where beam steering may be present. Accordingly, we form a cavity of length 75 cm, with 50 cm ROC mirrors (Research Electro Optics). No beam steering is detected with this geometry (either by the CCD camera, or in the resulting profiles). Qualitatively, this geometry tends to recentre deviated beams, whereas the more planar geometry is not as effective. The 50 cm ROC cavity yields ring-down times of approximately 12 μs, corresponding to mirror reflectivities of about 0.9998, or equivalently about 2500 round-trips by the light inside the cavity during one Neperian decay time.

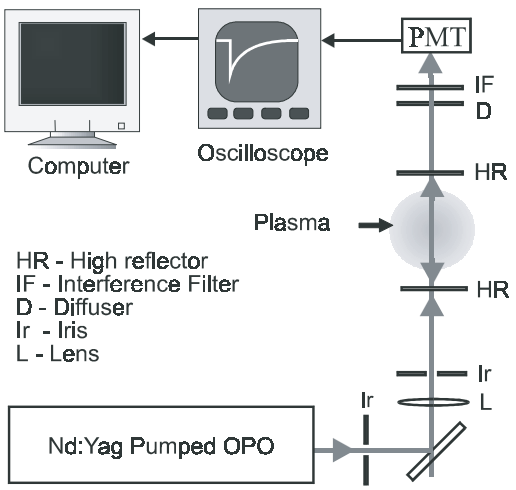

Figure 2. Schematic diagram of CRDS set-up. The ring-down cavity has a length of 0.75 m, and uses mirrors of 2.54 cm diameter, and 0.5 m radius of curvature. An OPO is used as the light source, and a photomultiplier tube (PMT) detects the light exiting the cavity.

3.3. Electrical

We also determine the electron number density in the discharge by an electrical conductivity approach. We measure the discharge current and electric field, and use Ohm's law to compute the product of the average electron number density and column area. The electric field is determined by measuring the discharge voltage versus electrode separation. We write Ohm's law as $j = i/\text{area} = (n_e e^2/m_e \Sigma \nu_{eh})E$, where ν_{eh} is the average collision frequency between electrons and heavy particles. Because of the low ionization fraction ($\lesssim 10^{-5}$), ν_{eh} is dominated by collisions with neutrals, so we can write $\nu_{eh} \cong n_n g_e Q_{en}$, where $n_n = P/kT_g$ is the number density of neutrals, $g_e = (8kT_e/\pi m_e)^{0.5}$ is the thermal electron velocity, and Q_{en} is the average momentum transfer cross-section for electron–nitrogen collisions. We determine T_e by means of a CR model [17], with input parameters (vibronic ground state population and rotational temperature) obtained from the CRDS measurements. Q_{en} is determined as a function of T_e from tabulated values [18].

4. Results and discussion

4.1. N_2^+ ring-down spectra

N_2^+ ring-down spectra are recorded as a function of discharge current and position. We discuss the spectra in terms of measurement accuracy and detection sensitivity. Figure 3 shows measured and simulated absorption spectra in the vicinity of the (0, 0) bandhead of the first negative system. Rotationally resolved lines from the P and R branches are visible. The lines are identified using tabulated line locations [19, 20], and are labelled with the angular momentum quantum

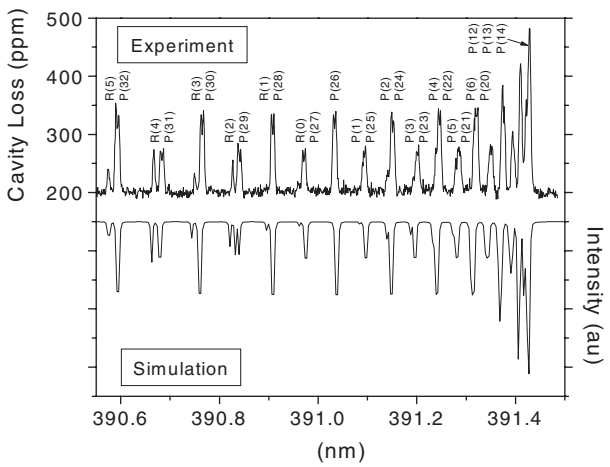

Figure 3. Measured and simulated N_2^+ absorption spectra near the (0, 0) bandhead of the first negative system. Lines from the P and R branches are identified.

number N″ of the lower state. The displayed spectrum is recorded along the discharge centreline, at a current of 187 mA, and averages 16 shots at each wavelength. The experimental spectrum is plotted in terms of single-pass cavity loss and illustrates the high sensitivity attainable with the CRDS technique. The cavity loss is the sum of mirror reflective loss and sample absorptive loss. (The Rayleigh scattering losses are computed to be negligible.) Near the bandhead, the signal is ∼280 ppm per pass, the baseline reflective loss is ∼200 ppm per pass, and the baseline noise is ∼5 ppm per pass, so that the signal-to-noise (S/N) ratio is ∼56. The S/N ratio suggests an absorbance-per-pass sensitivity of ∼1 ppm, which corresponds to a detection limit of about 7×10^{10} cm^{-3} for N_2^+ ions at our experimental conditions. The baseline reflective loss of ∼200 ppm per pass corresponds to a mirror reflectivity of ∼0.9998 which is in accord with the manufacturer's specifications.

Figure 4 shows an expanded view of the P(28) and R(1) lines after baseline subtraction. Fitted Voigt peaks (constrained to have the same shape and width) are shown with solid lines, and their sum is shown with a dotted line. For the P(28) lines, the doublet structure due to the unpaired electron is apparent. The fit yields a doublet spacing of 0.005 nm, in good agreement with the literature [19, 20]. The R(1) lines are close to the detection limit and correspond to a N_2^+ X state population of about 10^{10} cm^{-3}. Their splitting is much less than the linewidths and is not resolved. The fitted FWHM of each peak is 0.0042 nm, or 7.9 GHz, which is consistent with an expected thermally broadened linewidth of ∼7 GHz and a measured laser linewidth of ∼4 GHz. Our calculations indicate that for these linewidths and absorption parameters, a measurement of the area of an absorbing feature will be negligibly affected by finite laser bandwidth [13]. Note that unlike in conventional absorption, such an assumption is not always correct in CRDS. The assumption was verified in the present work by fitting progressively earlier parts of the ring-down signal and confirming that the apparent absorbance remains constant.

4.2. Concentration profiles

We obtain spatial profiles of the N_2^+ concentration by displacing the discharge perpendicularly to the optical axis. CRDS is a path-integrated technique and the discharge has axial symmetry. We verify the symmetry of the discharge by performing measurements with the plasma rotated by 90°, and find that the cases have <2% deviation. We use an Abel inversion to recover the radial N_2^+ concentration profile. The concentration measurements are based on the (frequency integrated) area of the lines P(9)–P(17) in the (0, 0) bandhead vicinity. We use tabulated line strengths from [19, 20]. Figure 5 shows concentration profiles determined for different values of current (i = 52, 97, 142 and 187 mA). We find peak (centreline) N_2^+ concentrations of 7.8×10^{11}, 1.5×10^{12}, 2.4×10^{12} and 3.6×10^{12} cm^{-3} for i = 52, 97, 142 and 187 mA, respectively. The shape of the concentration profile remains approximately uniform at the different conditions, though we observe that the radial half-maximum values increase slightly with current. We find radial half-maximums of 0.80, 0.82, 0.93, and 1.05 mm for i = 52, 97, 142 and 187 mA, respectively.

The error bars on N_2^+ concentration represent one standard deviation (1σ). They primarily arise from the uncertainties in relating the measured population of several rotational levels in the ground vibronic state, to the overall population of N_2^+. Because the discharge is out of equilibrium, this determination depends on the how the rotational, vibrational, and electronic energy levels are populated. The rotational levels are equilibrated at the gas temperature owing to fast collisional relaxation. CRDS measurements in this discharge and emission measurements in similar glow discharges [1] indicate that the rotational temperature profile is significantly wider than the charged species concentration profiles, so we assume a constant rotational temperature. The rotational temperatures used in the analysis are obtained from Boltzmann plots, and are T_r = 3100, 3600, 4150 and 4700 K for currents of i = 52, 97, 142 and 187 mA, respectively. The vibrational and electronic energy levels are out of equilibrium, and a CR model [17] is used to determine the fraction of the population in the ground vibronic state, and predicts 0.37 ± 0.02, 0.35 ± 0.02, 0.33 ± 0.02 and 0.31 ± 0.02 for i = 52, 97, 142 and 187 mA, respectively. Combining the rotational temperature uncertainties with those from the CR model and those from the Abel inversion (∼4%), results in an overall experimental uncertainty in concentration of ∼10%.

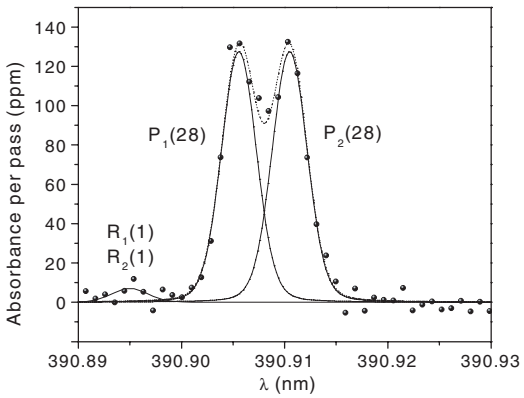

Figure 4. Expanded view of P(28), and R(1) lines from figure 3(*a*). Background absorption has been subtracted. Voigt peaks fitted to the doublet are shown with solid lines, while their sum is shown with a dotted line.

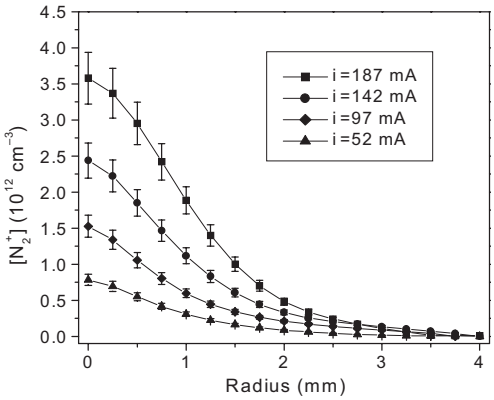

Figure 5. Radial concentration profiles of N_2^+ measured by CRDS in an atmospheric pressure glow discharge. Experimental data points are joined with line segments for visual clarity.

Table 1. Comparison of electron number densities (at the radial half-maximum) found by CRDS to those found by electrical measurement. The final column gives the ratio of the measured electron number density to the concentration corresponding to an LTE plasma at the same gas temperature.

i (mA)	$n_{\text{e-CRDS}}$ (cm^{-3})	$n_{\text{e-Elec}}$ (cm^{-3})	$n_{\text{e-CRDS}}/n_{\text{e-Elec}}$	$n_{\text{e-CRDS}}/n_{\text{e-LTE}}$
52	$4.1 \pm 0.4 \times 10^{11}$	$3.8 \pm 0.4 \times 10^{11}$	1.08 ± 0.16	2.8×10^{4}
97	$8.2 \pm 0.8 \times 10^{11}$	$7.8 \pm 0.8 \times 10^{11}$	1.05 ± 0.16	980
142	$1.37 \pm 0.14 \times 10^{12}$	$1.42 \pm 0.14 \times 10^{12}$	0.96 ± 0.14	48
187	$2.1 \pm 0.2 \times 10^{12}$	$2.0 \pm 0.2 \times 10^{12}$	1.06 ± 0.16	5.6

The spatial resolution of our measurements is determined by the spatial step-size (0.2 mm). To justify this claim, we need to verify that the dimension of our laser beam waist does not influence the measured spatial profiles. The simulations by Spuler *et al* [16] indicate that our expected beam waist is approximately 160–320 μm, depending on the level of mode matching achieved. Deconvoluting the broader case has an effect of only about 1% (0.02 mm) on the measured profiles, which is negligible compared to the spatial step-size. Therefore the resulting spatial resolution is about 0.2 mm.

4.3. Comparison with electrical measurements

The ratio of the measured discharge current and electric field yields the product of the average electric conductivity with the discharge area. Inferring the electron density from the electric conductivity requires T_e, which we infer from the measured gas (rotational) temperature and ion concentrations using a CR model [17]. The dependence of ion concentration on T_e is steep, and for all experimental conditions we find values of T_e in the range 9400–9600 K. For $T_e = 9500$ K, we find an average momentum transfer cross-section $Q_{en} = Q(\text{e–N}_2) = 1.08 \pm 0.05 \times 10^{-15}\,\text{cm}^2$ [18]. For each discharge condition, we assume the electron number density profile has the same shape as the ion profile found from CRDS, and determine the electron number density at the radial half-maximum accordingly. The objective is to compare the electron number density derived from electrical measurement with a value derived from the ion concentration measurements. At our conditions, the CR model predicts that 96, 93, 89 and 85% of ions are N_2^+, and the remainder is N^+, for $i = 52$, 97, 142 and 187 mA, respectively. By charge balance, the sum of the N_2^+ and N^+ concentrations equals the electron number density. We convert the N_2^+ concentration profiles to electron number density profiles using these percentages. The electron number densities (at the radial half-maximum) found by electrical measurements are compared with those inferred from the CRDS ion measurements in table 1. The values are plotted in figure 6. The uncertainty in the electrical measurement (10%) is primarily from uncertainties in the momentum transfer cross-section (5%), the discharge area (4%), and the average gas temperature (8%). Column 4 of table 1 shows that the electron number densities found from optical and electrical measurements overlap within their error bars. This excellent agreement gives us confidence in our results for the electron number density.

The ratio of the measured electron number density (at the radial half-maximum) to the LTE electron number density at the corresponding gas temperature is shown in column 5 of table 1. The measured ion and electron concentrations in the discharge are significantly higher than those corresponding to LTE conditions at the same gas temperature. The results quantify the degree of ionizational nonequilibrium in the discharges. At higher values of discharge current the LTE concentration of charged species rises steeply, so that the ratio of measured concentration to LTE concentration reduces. Related work in our laboratory has shown that by flowing the gas more quickly, comparable electron densities may be achieved with lower gas temperatures [1].

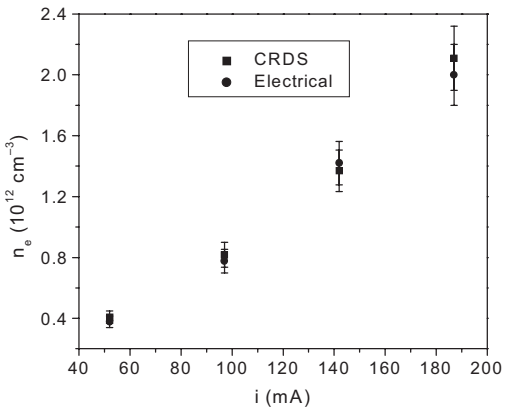

Figure 6. Electron number densities (at the radial half-maximum) as a function of discharge current. Number densities are derived from CRDS ion measurements (■), and from electrical measurement (●).

5. Conclusion

Spatial profiles of N_2^+ concentration have been measured in an atmospheric pressure nitrogen glow discharge by CRDS. Special care in the selection of cavity geometry is needed in the atmospheric pressure plasma environment. Sub-millimetre spatial resolution and sub-ppm concentration sensitivity have been achieved. The signal-to-noise ratio suggests a detection limit of about $7 \times 10^{10}\,\text{cm}^{-3}$ for N_2^+ ions at our experimental conditions. Using a CR model we infer electron number densities from the measured ion profiles. The values of electron number density found in this way are consistent with those found from electrical measurements. The spectroscopic technique is clearly favourable, because it offers spatial resolution and does not require knowledge of other discharge parameters. The measurements indicate that the atmospheric pressure discharges studied here are two-temperature plasmas with electron number densities elevated with respect to equilibrium, which is characteristic of glow-discharge plasmas.

Acknowledgments

This work was primarily funded by the Director of Defense Research & Engineering (DDR&E) within the Air Plasma Ramparts MURI program managed by the Air Force Office of Scientific Research (AFOSR).

References

[1] Yu L, Laux C O, Packan D M and Kruger C H 2002 *J. Appl. Phys.* **91** 2678–86
[2] Laux C O *et al* 1999 Ionization mechanisms in two-temperature air plasmas *30th AIAA Plasmadynamics and Lasers Conf. (Norfolk, VA)*
[3] Quandt E, Kraemer I and Dobele H F 1999 *Europhys. Lett.* **45** 32–7
[4] Grangeon F *et al* 1999 *Plasma Sources Sci. Technol.* **8** 448–56
[5] Kessels W M M *et al* 2001 *J. Vac. Sci. Technol.* A **19** 467–76
[6] Schwabedissen A, Brockhaus A, Georg A and Engemann J 2001 *J. Phys. D: Appl. Phys.* **34** 1116–21
[7] Booth J P, Cunge G, Biennier L, Romanini D and Kachanov A 2000 *Chem. Phys. Lett.* **317** 631–6
[8] Kotterer M, Conceicao J and Maier J P 1996 *Chem. Phys. Lett.* **259** 233–6
[9] Aldener M, Lindgren B, Petersson A and Sassenberg U 2000 *Phys. Scr.* **61** 62–5
[10] Busch K W and Busch A M (eds) 1999 *Cavity-Ringdown Spectroscopy* (*ACS Symp. Series*) vol 720 (Washington, DC: American Chemical Society)
[11] Berden G, Peeters R and M G 2000 *Int. Rev. Phys. Chem.* **19** 565–607
[12] Zalicki P and Zare R N 1995 *J. Chem. Phys.* **102** 2708–17
[13] Yalin A P and Zare R N 2002 *Laser Phys.* at press
[14] Siegman A E 1986 *Lasers* (Mill Valley: University Science Books)
[15] Thoman J W and McIlroy A 2000 *J. Phys. Chem.* A **104**, 4953–61
[16] Spuler S and Linne M 2001 *Appl. Opt.* at press
[17] Pierrot L, Yu L, Gessman R J, Laux C O and Kruger C H 1999 Collisional-radiative modeling of nonequilibrium effects in nitrogen plasmas *30th AIAA Plasmadynamics and Lasers Conf. (Norfolk, VA)*
[18] Shkarofsky I P, Johnston T W and Bachynski M P 1966 *The Particle Kinetics of Plasmas* (Reading, MA: Addison-Wesley)
[19] Michaud F, Roux F, Davis S P, Nguyen A-D and Laux C O 2000 *J. Mol. Spectrosc.* **203** 1–8
[20] Laux C O *et al* 2001 *J. Quant. Spectrosc. Radiat. Transfer* **68** 473–82